Title: Early and widespread engagement of the cerebellum during hippocampal epileptiform activity

Format: Brief Communication

Authors: M.L. Streng[1], B.W. Kottke[1], E.M. Wasserman[1], L. Zecker[1], L. Luong[1], T.J. Ebner[1], E. Krook-Magnuson[1]

Key words: Temporal Lobe Epilepsy, See-Shell, Purkinje cells, IED, focal epilepsy

Corresponding Author:

[1]Department of Neuroscience, University of Minnesota, Minneapolis, MN, USA.

Correspondence: Martha Streng, Ph.D.

Department of Neuroscience

University of Minnesota

Jackson Hall, room 6-145

321 Church Street SE

Minneapolis, MN 55455

Phone: 612-624-4494

Email: stren021@umn.edu

Title: Early and widespread engagement of the cerebellum during hippocampal epileptiform activity

Abstract

Despite research illustrating the cerebellum may be a critical circuit element in the epilepsies, remarkably little is known about cerebellar engagement during seizures. We therefore implemented a novel method for repeated imaging of the cerebellum in awake, chronically epileptic animals. We found widespread changes in cerebellar calcium signals during behavioral seizures *and* during hippocampal seizures that remained electrographic only, arguing against cerebellar modulation simply reflecting motor components. Moreover, even brief interictal spikes produced widespread alterations in cerebellar activity. Changes were noted in the anterior and posterior cerebellum, along the midline, and both ipsilaterally and contralaterally to the seizure focus. Remarkably, changes in the cerebellum also occurred *prior* to any noticeable change in the hippocampal electrographic recordings, suggesting a special relationship between the cerebellum and hippocampal epileptiform activity. Together these results underscore the importance of the cerebellum in epilepsy, warranting a more consistent consideration of the cerebellum when evaluating epilepsy patients.

Main text

The cerebellum, though often neglected in epilepsy research and clinical care alike, can be impacted by epilepsy and seizures [1-8], and vice versa [9-13]. However, studies examining the cerebellum during seizures in patients are very limited[1,2], and even in rodents have largely been limited to local field potentials (LFP) or single unit recordings [1,3-5]. While single unit recordings have overcome potential volume-conduction concerns associated with LFP recordings, and have convincingly demonstrated that the cerebellum can "seize" [3,4,14], the extent of such modulation is unknown. Single unit recordings have also not allowed for consideration of modulation across repeated spontaneous seizure events in chronically epileptic animals, which is necessary to determine reliability of any potential changes.

We therefore adapted conformant See-Shell [15] technology to allow chronic, widefield, monitoring of the cerebellar cortex [16], including lobules IV-VII (**Supplementary Figure 1**). Sparse expression of GCaMP6s selectively in Purkinje cells allowed single cell resolution, and 1-photon imaging allowed simultaneous monitoring of both somatic and dendritic aspects [16] (**Supplementary Fig. 1**). Unsupervised spatial independent component analysis provided unbiased segregation of the widefield Ca^{2+} signals into functional domains, which appeared as parasagittal bands and, separately, Purkinje cell somata (**Supplementary Fig. 1**, Supplementary Methods) [16].

To prevent direct damage to the cerebellum and to have a known site of injury, we utilized the unilateral intrahippocampal kainate mouse model, in which the initial injury produces chronic epilepsy with hallmarks of unilateral temporal lobe epilepsy, including hippocampal sclerosis [17]. Repeated imaging sessions in chronically epileptic animals (with concurrent hippocampal LFP recordings from the hippocampus near the presumed seizure focus) allowed us to capture even relatively rare spontaneous seizure events: over 1,116 three minute recording stacks, across 71 recording sessions from 6 animals, we successfully imaged the cerebellum during 11 spontaneous, recurrent, overtly behavioral, seizures

(**Figure 1**). These seizures reached at least Stage 3 on the Racine Scale (including minimally forelimb clonus) [18].

Ca^{2+} activity in the cerebellum was clearly modulated by overtly behavioral temporal lobe seizures (**Figure 1**). In fact, seizures evoked widespread changes across the entire imaged cerebellum, including medial portions as well as lateral cerebellum (including Simplex and Crux I; **Supplementary Figure 1**), both ipsilateral and contralateral to the seizure focus (**Fig. 1A,B**). At the onset of behavioral seizures, even prior to the onset of noticeable motor engagement, there was a marked increase in Purkinje cell activity, visible in both the parasagittal and somatic domains (**Fig. 1A-C; Supplementary Figure 2**). As the seizures progressed, this hyperactivity gave way to marked hypoactivity, typically starting first in the anterior cerebellum and progressively incorporating the more posterior aspects (as shown in the heat maps in **Fig.1A,B** and in **Supplementary Video 1**). During periods of hippocampal LFP postictal depression, the cerebellum was essentially silent (**Fig.1A,B, D, Video 1**). This cerebellar quiescence could occur at the time of seizure offset (i.e., at the time of hippocampal postictal depression) (**Fig. 1A**), or, more commonly, actually precede hippocampal LFP depression (**Fig. 1B, D**).

While seizures are often associated with hypersynchronous activity, and while activity overall in the cerebellum was increased during seizures, we did not find, at the time resolution calcium activity affords, evidence for widespread increases in correlated calcium activity in the cerebellum during seizures relative to interictal periods (**Supplementary Figure 3**).

Together, these data suggest that i) the cerebellum undergoes widespread modulation during seizures, but not dramatic increases in correlations, 2) the widespread modulation during seizures cannot be explained simply by the motor components of seizures, 3) that modulation of the cerebellum is not static, nor uniform, but rather goes through phases as a behavioral seizure progresses, and 4) hints that cerebellar modulation may even precede noticeable changes in the hippocampal LFP signal. However, as these are large behavioral seizures, potential caveats exist. We therefore turned to more subtle hippocampal epileptiform events (**Figure 2**), including electrographic-only seizures with no apparent motor alterations (**Supplementary Fig. 4**) and brief interictal spikes (interictal epileptiform discharges: IEDs). This allowed for dissociation of possible motor contributions to cerebellar alterations, and provided a tight temporal window to examine cerebellar alterations in relationship to hippocampal LFP.

We examined 647 hippocampal electrographic-only seizure events across 6 mice (**Figure 2**). As these events had variable durations, we aligned calcium signals to either the onset or the offset of the electrographic seizure event (**Fig. 2A-C** and **Fig. 2 D-F**, respectively). As with large, overtly behavioral, seizures, electrographic-only events were associated with widespread changes in the cerebellum, including medial portions (vermis; **Fig. 2A, 2D**) as well as lateral cerebellum (**Fig. 2A, 2D**), both contralateral (F**ig. 2C top, 2F top**) and ipsilateral (**Fig. 2C bottom, 2F bottom**) to the seizure focus, and was visible in both the parasagittal domains and in individual Purkinje cell somata (**Supplementary Fig. 2**). Effects were generally more prominent in the more posterior aspects of the imaging window (**Figure 2A-F**).

Remarkably, immediately *prior* to electrographic seizure onset, calcium signals were decreased across the cerebellum (**Fig. 2A-C, G**), suggesting that either the cerebellum is producing a seizure-prone state, or, minimally, that the cerebellum is an effective readout of a seizure-prone state. Notably, these changes in the cerebellum occurred prior to any noticeable change in the hippocampal LFP (**Fig. 2B**).

Seizure offset showed an inverse profile, with a marked rebound in cerebellar signals as the seizure terminated (**Fig. 2D-G**). These findings held for both male and female animals (**Supplementary Fig. 5**).

IEDs are very brief events, lasting on average ~100ms in our recordings (**Fig. 2K**). Despite this brief duration, they were also associated with dramatic changes in calcium signals across the cerebellum (**Fig. 2H-L**). As with electrographic seizure events, cerebellar modulation was bidirectional, with an initial decrease and then a rebound following the IED. Astoundingly, even for IEDs, changes occurred in the cerebellum *prior* to any apparent changes in the hippocampal LFP (**Fig. 2K**). Therefore, even brief, temporally constrained, hippocampal epileptiform events are associated with widespread cerebellar changes, *and* these changes can occur immediately *prior* to hippocampal LFP changes. This is even more striking when considering the slow temporal dynamics of Ca^{2+} imaging compared to the much faster temporal readout of LFP; this leaves no doubt that the cerebellar changes precede by hundreds of milliseconds the hippocampal LFP changes marking an IED.

Cerebellar alterations (specifically gray matter loss) are associated with an increased risk of Sudden Unexpected Death in Epilepsy (SUDEP)[19]. We examined IED related cerebellar changes with respect to two time points. First, we examined IEDs with respect to an approaching behavioral seizure (**Fig. 2M**). The closer in time to a large behavioral seizure, the more muted the IED cerebellar response (**Fig. 2N**). Additionally, we had enough chronic recordings from one animal that eventually succumbed to a putative SUDEP event to examine cerebellar activity during IEDs in relationship to death. Here too we found a decrease in cerebellar IED responsiveness (**Fig. 2O-P**), suggesting that cerebellar IED responsiveness can serve as a measure of disease severity on both acute (minutes) and more extended (days-months) time scales.

While the cerebellum is often neglected in epilepsy research, a robust body of literature has indicated that it can be engaged by a variety of seizure types, including temporal lobe seizures (for reviews, see references [1,2]). However, the extent of cerebellar modulation was unknown, and concerns about potential motor contributions lingered. Our results illustrate that widespread areas of the cerebellum (indeed, the entire imaging field of view -- encompassing anterior and posterior cerebellum, and medial and lateral cerebellum) are modulated by large behavioral seizures, and also by seizures observable in the hippocampal LFP that were not accompanied by overt motor manifestations. Indeed, even brief hippocampal IEDs were accompanied by marked cerebellar alterations. These results highlight that the cerebellum should be considered as a potential key node in seizure networks. This is true for both translational research and, importantly, during clinical evaluations. The cerebellum is not a passive bystander during hippocampal seizures.

Despite its historic neglect, it may not be entirely surprising that activity in the cerebellum is altered during hippocampal epileptiform activity, as even IEDs can induce widespread neocortical changes[20]. Notably, however, such widespread modulation of the neocortex is in keeping with the hippocampal interictal spike *inducing* neocortical changes. Even calcium imaging from the contralateral hippocampus during IEDs illustrate changes during (specifically, an increase in inhibitory interneuron firing) and after (a decrease in pyramidal cell firing), rather than changes *prior* to the IED [21]. In contrast, our data illustrate that changes in the cerebellum can actually precede the hippocampal IED. This questions the order of cause-and-effect, or suggests that the cerebellum is particularly sensitive to hippocampal changes, such that even early hippocampal changes -- which are not yet discernable in the LFP [22] -- are

able to cause marked, widespread, cerebellar changes. Either scenario would be remarkable, and requires serious reconsideration of how the cerebellum is viewed in relationship to epileptiform activity.

The cerebellum is rarely believed to be the seizure focus, though a growing number of case reports underscore that the cerebellum can be ictogenic (reviewed in reference [1]). Additionally, the cerebellum is rarely included in a surgical workup for epilepsy patients. Increased monitoring may lead to increased observations of the cerebellum being engaged during epileptiform activity in clinical populations. Indeed, in a rare clinical depth recording from the cerebellum (in a patient with chronic epilepsy following encephalitis 7 years prior), strong and early engagement was recorded from the fastigial electrode [5], underscoring the clinical relevance of our findings. Indeed, our work highlights that the cerebellum should be considered as an area of interest even in cases where the seizure focus is believed to be well-defined. The cerebellum, and its early modulation, may also provide a means for seizure prediction or forecasting [23,24] with a very short temporal window, which would allow effective, time-restricted, interventions. Given that on-demand modulation of the cerebellum has been shown to inhibit seizures (for both absence and temporal lobe epilepsy [4,9,10,12]), this raises the possibility of both early seizure detection/prediction and closed-loop intervention occurring from cerebellar locations. In short, as the cerebellum shows early and widespread engagement during diverse forms of epileptiform activity, and as previous work has shown the cerebellum can also be a target for seizure control, the cerebellum should be considered as a potential critical node in seizure networks.

Figure 1

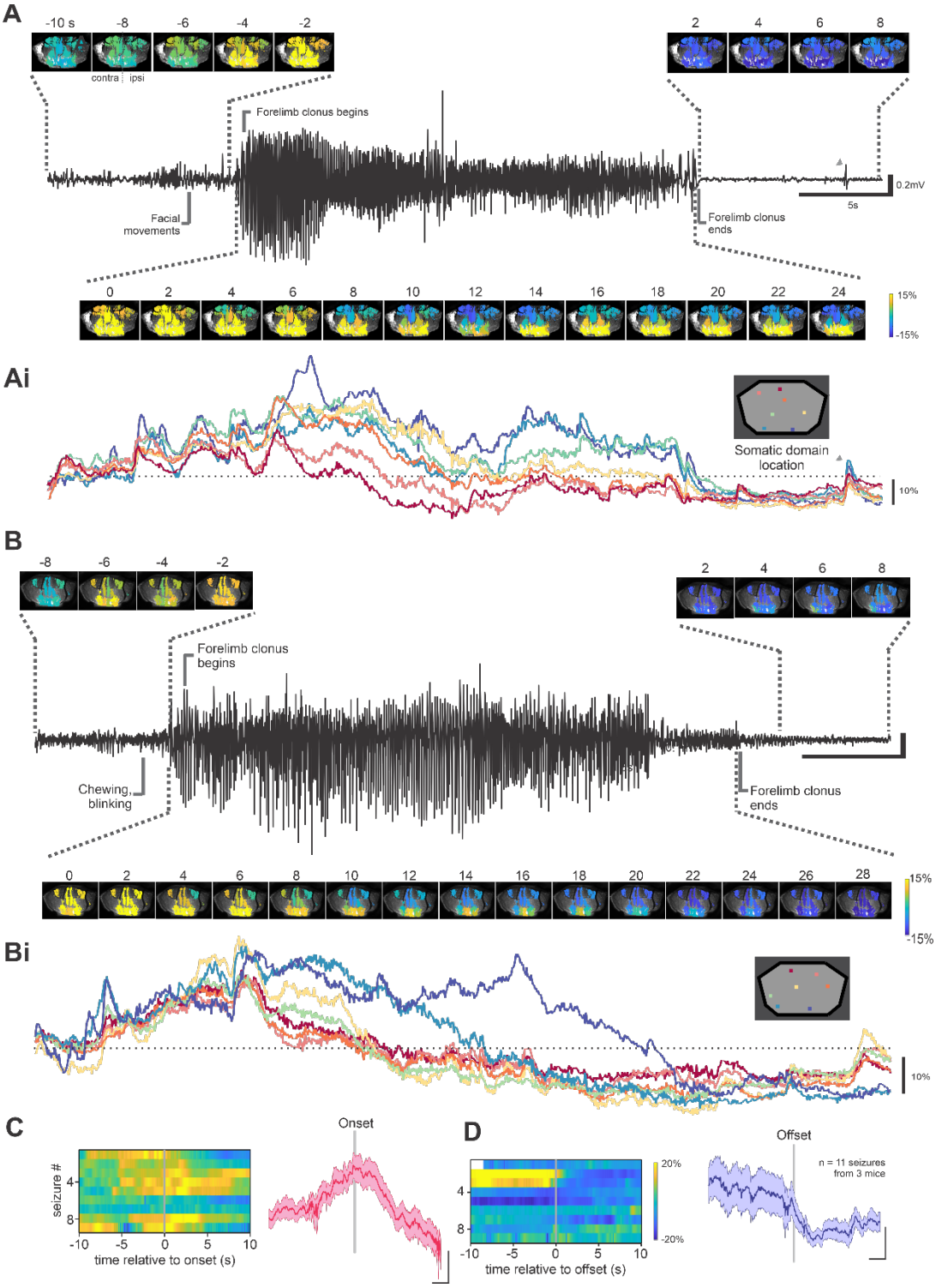

Figure 1. Widespread changes in cerebellar activity associated with overtly behavioral seizure events. A. Example recorded spontaneous behavioral seizure (LFP recorded from the dorsal hippocampus) and

associated changes in cerebellar parasagittal domains' calcium signals (heat maps). Note the increase that happens prior to the onset of large amplitude hippocampal spiking and the widespread decrease during hippocampal postictal depression. Ai. ΔF/F traces for example Purkinje cell somata, color coded by location. B. As in A, but for a different example seizure from a different example mouse. C. Relative activity levels at the time large amplitude spiking begins in the hippocampus. Each row represents a different behavioral seizure. Right: average ΔF/F. Shading: SEM. D. As in C, but aligned to the cessation of large amplitude spiking. Scale bars: A: 0.2mV, 5s; Ai: 10% ΔF/F; B: 0.1mV, 5s; Bi 10% ΔF/F; C,D: 5% ΔF/F, 2s.

Figure 2.

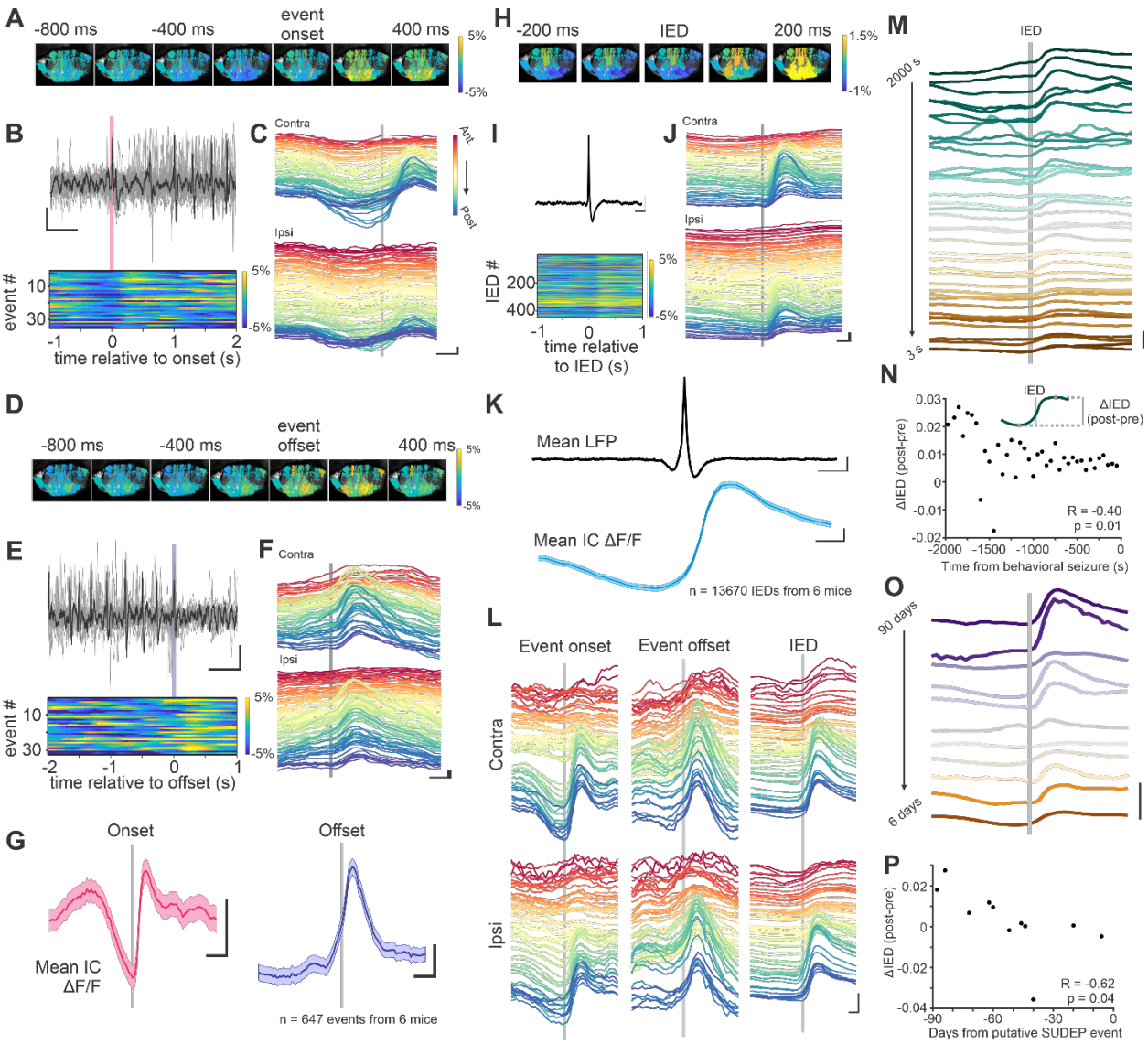

Figure 2. Electrographic events also cause early and widespread cerebellar changes.

A. Parasagittal domain changes in cerebellar calcium activity in an example mouse for one recording session, aligned to the time of electrographic-only seizure event onsets. B. Associated example hippocampal electrographic events (top), with one shown in black for easy visualization. Bottom: Cerebellar changes by event, averaged across the entire imaging window. C. Cerebellar calcium changes for this example animal and recording session averaged across events, by location within the cerebellum. Top: contralateral to the seizure focus; bottom: ipsilateral; warmer colors: anterior cerebellum. For A-C, note that the decrease in cerebellar activity actually precedes the first hippocampal spike. D-F. As in A for the same example animal and recording session, but aligned to

electrographic seizure offset. G: Average change in fluorescence (ΔF/F) aligned to onset (left) or offset (right) of events across the population. Shading: SEM. H-J. As in A-C, but for IEDs. K. Average hippocampal LFP IED (top) and associated average change in cerebellar calcium activity (bottom). Note that the decrease in average calcium activity begins >200 msec prior to any noticeable change in the hippocampal LFP (averaged across over 10,000 IEDs). L. Average cerebellar changes by location within the cerebellum for electrographic hippocampal seizure onset (left), offset (middle), and IEDs (right), illustrating significant cerebellar modulation ($p < 0.01$, Wilcoxon signed rank tests, see supplementary methods). Note that the IED changes, the preictial decrease followed by ictal onset and offset increase, and the generally larger engagement of the more posterior aspects of the imaged area are seen for both parasagittal and somatic domains (**Supplementary Figure 2**) and for both males and females (**Supplementary Figure 5**). M-P. The peri-IED change in cerebellar calcium signals becomes more muted as a behavioral seizure (M-N) or death (O-P) approaches. M: each line represents the average peri-IED cerebellar response relative to behavioral seizure onset, beginning 2000 sec prior to the seizure, in 50 second bins. N: Each dot represents the quantified peri-IED change from each line in M. O: Same as for M, but for an animal recorded over a three month period ending in a putative SUDEP event. Lines indicate the peri-IED cerebellar response in 2 day bins. P: same as for N, but for each line in O. Scale bars: B 0.5 s, 0.1mV. C 200 msec, 1% ΔF/F. E: 0.5 s, 0.1mV. F: 200 msec, 1% ΔF/F G: 500 msec, 0.5% ΔF/F. I: 200 msec, 0.1mV. J: 200 msec, 1% ΔF/F K: 200 msec, 0.1mV (top), 1% ΔF/F (bottom) L: 200 msec, 1% ΔF/F M: 5% ΔF/F O: 2% ΔF/F.

References

1. Streng, M.L., Froula, J.M. & Krook-Magnuson, E. The cerebellum's understated role and influences in the epilepsies. *Neurobiology of disease* **183**, 106160 (2023).
2. Streng, M.L. & Krook-Magnuson, E. The cerebellum and epilepsy. *Epilepsy & behavior : E&B*, 106909 (2020).
3. Kandel, A. & Buzsaki, G. Cerebellar neuronal activity correlates with spike and wave EEG patterns in the rat. *Epilepsy research* **16**, 1-9 (1993).
4. Krook-Magnuson, E., Szabo, G.G., Armstrong, C., Oijala, M. & Soltesz, I. Cerebellar Directed Optogenetic Intervention Inhibits Spontaneous Hippocampal Seizures in a Mouse Model of Temporal Lobe Epilepsy. *eNeuro* **1**(2014).
5. Niedermeyer, E. & Uematsu, S. Electroencephalographic recordings from deep cerebellar structures in patients with uncontrolled epileptic seizures. *Electroencephalography and clinical neurophysiology* **37**, 355-365 (1974).
6. Blumenfeld, H.*, et al.* Cortical and subcortical networks in human secondarily generalized tonic-clonic seizures. *Brain : a journal of neurology* **132**, 999-1012 (2009).
7. Kros, L.*, et al.* Synchronicity and Rhythmicity of Purkinje Cell Firing during Generalized Spike-and-Wave Discharges in a Natural Mouse Model of Absence Epilepsy. *Front Cell Neurosci* **11**, 346 (2017).
8. Kerestes, R.*, et al.* Patterns of subregional cerebellar atrophy across epilepsy syndromes: An ENIGMA-Epilepsy study. *bioRxiv* (2023).
9. Stieve, B.J., Richner, T.J., Krook-Magnuson, C., Netoff, T.I. & Krook-Magnuson, E. Optimization of closed-loop electrical stimulation enables robust cerebellar-directed seizure control. *Brain : a journal of neurology* (2022).
10. Streng, M.L., Tetzlaff, M.R. & Krook-Magnuson, E. Distinct Fastigial Output Channels and Their Impact on Temporal Lobe Seizures. *The Journal of neuroscience : the official journal of the Society for Neuroscience* **41**, 10091-10107 (2021).
11. Eelkman Rooda, O.H.J.*, et al.* Single-pulse stimulation of cerebellar nuclei stops epileptic thalamic activity. *Brain stimulation* **14**, 861-872 (2021).
12. Kros, L.*, et al.* Cerebellar output controls generalized spike-and-wave discharge occurrence. *Annals of neurology* **77**, 1027-1049 (2015).
13. Kros, L., Rooda, O.H., De Zeeuw, C.I. & Hoebeek, F.E. Controlling Cerebellar Output to Treat Refractory Epilepsy. *Trends in neurosciences* **38**, 787-799 (2015).
14. Fernandez-Guardiola, A., Manni, E., Wilson, J.H. & Dow, R.S. Microelectrode recording of cerebellar and cerebral unit activity during convulsive afterdischarge. *Experimental neurology* **6**, 48-69 (1962).
15. Ghanbari, L.*, et al.* Cortex-wide neural interfacing via transparent polymer skulls. *Nature communications* **10**, 1500 (2019).
16. Streng, M.L.*, et al.* Mesoscale Ca2+ imaging reveals networks of Purkinje cell dendritic and somatic modulation, with divergent roles of activity versus correlation during behavior. *bioRxiv*, 2023.2010.2005.561090 (2023).
17. Cavalheiro, E.A., Riche, D.A. & Le Gal La Salle, G. Long-term effects of intrahippocampal kainic acid injection in rats: a method for inducing spontaneous recurrent seizures. *Electroencephalography and clinical neurophysiology* **53**, 581-589 (1982).
18. Racine, R. Modification of Seizure Activity by Electrical Stimulation: II. Motor Seizure. *Electroencephalography and clinical neurophysiology* **32**, 281-294 (1971).
19. Allen, L.A.*, et al.* Cerebellar, limbic, and midbrain volume alterations in sudden unexpected death in epilepsy. *Epilepsia* **60**, 718-729 (2019).

20. Gelinas, J.N., Khodagholy, D., Thesen, T., Devinsky, O. & Buzsaki, G. Interictal epileptiform discharges induce hippocampal-cortical coupling in temporal lobe epilepsy. *Nat Med* **22**, 641-648 (2016).
21. Muldoon, S.F.*, et al.* GABAergic inhibition shapes interictal dynamics in awake epileptic mice. *Brain : a journal of neurology* **138**, 2875-2890 (2015).
22. Wenzel, M., Hamm, J.P., Peterka, D.S. & Yuste, R. Acute Focal Seizures Start As Local Synchronizations of Neuronal Ensembles. *The Journal of neuroscience : the official journal of the Society for Neuroscience* **39**, 8562-8575 (2019).
23. Andrzejak, R.G.*, et al.* Seizure forecasting: Where do we stand? *Epilepsia* **64 Suppl 3**, S62-S71 (2023).
24. Jirsa, V.K., Stacey, W.C., Quilichini, P.P., Ivanov, A.I. & Bernard, C. On the nature of seizure dynamics. *Brain : a journal of neurology* **137**, 2210-2230 (2014).

Supplementary Materials

Supplementary Methods

Previous work using calcium imaging has yielded important insights into seizures and epileptic networks [1-20]. Largely due to technical considerations, these studies have often focused on a small imaging window, reduced preparations, and/or evoked, rather than spontaneous, seizure events. To examine activity in the cerebellum, across a large area of the cerebellum, during spontaneous epileptiform activity, including rare overtly behavioral seizures, we developed a method to allow concurrent hippocampal local field potential (LFP) monitoring with repeated widefield cerebellar imaging in awake animals (Supplementary Figure 1). This allowed examination of Purkinje cell calcium signals with respect to interictal epileptiform discharges (IEDs), electrographic seizure events, and overtly behavioral seizures, as detailed below. All were spontaneous epileptiform events in chronically epileptic animals.

Ethical approval

All experimental protocols were approved by the University of Minnesota's Institutional Animal Care and Use Committee.

Animals

For all experiments, mice were bred in-house and had *ad libitum* access to food and water in all housing conditions. Mice expressing the Ca^{2+} indicator GCaMP6s selectively in Purkinje cells were generated by crossing mice expressing Cre selectively in Purkinje cells in the cerebellum (B6.Cg-Tg(Pcp2-cre)3555Jdhu/J; Jackson Laboratory stock 010536)[21] with floxed-STOP GCaMP6s mice (B6.Cg-Igs7tm162.1(tetO-GCaMP6s,CAG-tTA2)Hze/J; Jackson Laboratory stock 031562)[22]. The resulting PcP2-GCaMP6s crosses had expression of GCaMP6s restricted to Purkinje cells, and in a sparse manner, as reported previously[23]. This allowed for single cell resolution of Purkinje cells at the wide-field level. Until implantation, animals were housed in standard housing conditions in the animal facility at the University of Minnesota. Following implantation, animals were singly housed in investigator managed housing on a 12-hour reverse light/dark cycle. A total of n = 6 mice of both sexes (n = 3 M, n = 3 F) were utilized in this study.

Surgical procedures

Epilepsy induction

Procedures for epilepsy induction using the mouse unilateral intrahippocampal kainic acid model of TLE largely followed previously published protocols [24-29]. Specifically, animals postnatal day 45 or greater were injected with 100nL kainic acid (KA, Tocris Biosciences) unilaterally into the right dorsal hippocampus (2.0 mm posterior, 1.25 mm right, 1.6 mm ventral from bregma) under isoflurane anesthesia (1.5-2%) as done in our previous work[28,29]. Animals were removed from isoflurane within five minutes post injection[30]. In this model, spontaneous

recurrent electrographic seizures emerge from the damaged hippocampus, providing a strong model of pharmocoresistant [31,32] temporal lobe epilepsy with hippocampal sclerosis [25,31,33,34]. Post-operative care consisted of recovery from anesthesia on a heating pad with regular visual inspection, followed by daily post-operative monitoring for a minimum of three days to inspect comfort level and healing of the surgical site. Neopredef powder was applied to the closed incisions as a topical antibiotic and analgesic. Only animals that showed spontaneous electrographic hippocampal seizures weeks after KA injection were included for simultaneous cerebellar imaging and hippocampal LFP monitoring.

Implantation

Cerebellar imaging windows were fabricated as described previously[23]. Implants consist of a small section of PET film affixed to a 3D-printed window frame, designed to conform to the contours of the skull, and a separate 3D-printed head fixation implant, which contained three holes tapped using an 0-80 hand tap for securing to a titanium headplate during the implantation surgery. A minimum of 2 weeks post KA injection, mice underwent implantation procedures[23] under isoflurane anesthesia. Buprenorphine ER (1mg/kg) and Dexamethasone (2mg/kg) were administered subcutaneously for analgesia and inflammation, respectively. The scalp was removed to expose the skull over the dorsal surface of both the cerebral and cerebellar cortices, and a large craniotomy matching the external profile of the cerebellar window frame was performed, exposing lobules IV/V, VI, and VII of the cerebellar cortex. The window was placed over the cerebellar cortex and bonded to the skull using Metabond dental cement (C&B Metabond, Parkell Inc.). Following window implantation, a twisted wire bipolar (local reference, differential) electrode (PlasticsOne) was stereotactically implanted ipsilateral to the site of KA (at 2.6 mm posterior, 1.75 mm right, 1.6 mm ventral from bregma) and secured with Metabond. The head fixation implant was next placed on the skull over the dorsal cerebral cortex and secured using Metabond. A custom titanium headplate was screwed onto the previously tapped holes in the head fixation implant, and the entire space between the window and headplate was filled with dental cement to protect the window from the external environment. A 3D-printed cap was attached to the titanium headplate to protect the PET surface. Post-operative care consisted of recovery from anesthesia on a heating pad with regular visual inspection, followed by daily post-operative monitoring for a minimum of three days to assess comfort level and healing of the surgical site. Animals were allowed to recover a minimum of five days prior to simultaneous cerebellar imaging and hippocampal LFP monitoring.

Simultaneous fluorescence imaging and hippocampal LFP monitoring

During imaging sessions, mice were head fixed on a freely moving disk treadmill to allow for spontaneous locomotion (Supplementary Figure 1). Awake, mesoscale cerebellar imaging was performed under an epifluorescence microscope (Nikon AZ100) with a 2X objective, as described previously[23]. Using a digital zoom, the field of view was adjusted to image the dorsal cerebellum, with the focal plane adjusted to allow for resolution of both Purkinje cell dendrites and somata. Dual wavelength illumination was used to capture both calcium-dependent (470 nm, blue light) and calcium-independent (405 nm, violet light) GCaMP6s signals on consecutive frames by a Cairn OptoLED driver (Cairn OptoLED, P1110/002/000; P1105/405/LED, P1105/470/LED). Calcium-dependent and calcium-independent signals were sampled by

alternating the illumination of the LEDs, as described previously[23,35-37]. Single-photon fluorescence images were captured at a frequency of 20 frames per second, 18 ms exposure, using a high-speed CMOS camera (ORCA-Flash4.0 V3, Hamamatsu photonics) controlled with MetaMorph. Behavior was monitored and recorded using a high-speed IR-sensitive CMOS camera (Blackfly, FLIR systems) under infrared illumination that did not affect concurrent calcium imaging. Synchronization of the behavior and microscope cameras was controlled by a series of TTL pulses delivered by Spike2 software and a CED power 1401 data acquisition system (Cambridge Electronic Design). Hippocampal LFP was recorded via electrical patch cords through an electrical commutator (PlasticsOne), amplified (Brownlee) and digitized (National Instruments). The TTL pulses controlling the behavior and microscope cameras were simultaneously recorded, allowing for the alignment of the Hippocampal LFP data to the cerebellar imaging data. The timing of spontaneous behavioral seizures, electrographic events, and interictal spikes were determined offline using our custom in house software, as described previously [28,29,34,38,39]. Spontaneous overt, behavioral seizures were confirmed using the behavioral monitoring videos. Mouse forepaw position was labeled using DeepLabCut for markerless behavioral tracking[40] to determine movement relative to hippocampal epileptiform activity.

Spatial independent component analysis

The preprocessing of cerebellar imaging data and determination of Purkinje cell spatial independent components (ICs) largely follows our previous methods[23,36,41-43]. Briefly, the first 10 seconds of each imaging stack data were removed to eliminate the initial rundown of the calcium fluorescence signal. Calcium-independent signals were removed by deinterleaving the 470 nm and 405 nm frames and subtracting the 405 nm signal, as described previously [35-37,41,44,45], followed by standard motion correction using co-registration [23,36]. The $\Delta F/F_{avg}$ (listed simply as of ΔF/F throughout) for each pixel was computed, with F_{avg} representing the mean corrected calcium-dependent signal across the recording stack. The resulting preprocessed imaging stacks were concatenated for a given recording day. Concatenated stacks were compressed using singular value decomposition (SVD), retaining the first 1000 principal components, which maintains important features of the full-rank data while drastically reducing the necessary computing time [43,46]. Spatial ICA was performed on the compressed dataset, and significant Purkinje cell ICs were determined using thresholding, and visually inspected for artifacts, as described previously[23]. As observed previously[23], cerebellar signals consisted of either parasagittal [47-51] or somatic domains[23] (Supplementary Figure 1).

Analysis of cerebellar modulation during epileptiform activity

For recording days with spontaneous overt, behavioral seizures, we aligned the ΔF/F of each cerebellar IC to seizure onset (defined for this purpose as the first large amplitude LFP spike) and offset (defined for this purpose as the last large amplitude LFP spike prior to onset of post-ictal depression) to determine the timing of cerebellar modulation. For visualization purposes, these ΔF/F signals were converted into a heat map for each parasagittal IC, and displayed at the appropriate spatial location on a map of the imaging window (as shown in Fig. 1A). For additional visualization of individual events, the ΔF/F of each IC over time was separated by the side relative to the seizure focus (i.e. the KA injected hippocampus), binned, and color-coded

based on the anterior-posterior positioning of the IC center (illustrated e.g. in Fig. 1Ai, Bi, Supplementary Figure 2Ai, Bi). The average ΔF/F of all cerebellar ICs across the population aligned to events was additionally computed. For illustrative purposes, this signal was converted into a heat map of average ΔF/F across all ICs for each event as shown in Fig. 1C-D). This was averaged across all recorded events to generate a global population average of calcium dynamics relative to seizure onset and seizure offset (line traces in Fig. 1C-D). A subset of behavioral seizures began just before the onset or ended just after the offset of an imaging stack, and were excluded from the respective population averaging. For hippocampal electrographic only events, the ΔF/F of each cerebellar IC was similarly aligned, binned, and averaged based on the onset or offset of electrographic events. Similar additional processing was completed for electrographic only events as were done for overtly behavioral seizures, as described above, including mean population traces by averaging across all cerebellar ICs, all recording days, and all mice. Similar procedures were used to determine cerebellar modulation relative to interictal epileptiform discharges (IEDs), with the ΔF/F of each IC aligned to the peak of the IED event in the hippocampal LFP. Cerebellar responses to IEDs were calculated by comparing the pre-IED ΔF/F (250ms before IED) and immediately post-IED ΔF/F (250ms after IED). These were then averaged across IEDs by 50 second bins relative to behavioral seizure onset (Fig. 2M-N) or by 2 day time bins relative to putative SUDEP event (Fig. 2O-P). Changes relative to behavioral seizure onset and/or putative SUDEP event were then examined using Pearsons' correlations.

Spatial correlation analysis

In order to quantify potential changes in correlated activity across ICs relative to seizure activity, IC ΔF/F data was separated into one of five epochs: interictal periods (defined as periods > 5 seconds from the onset or offset of an overtly behavioral seizure), preictal periods (up to 5 seconds before the onset of an event), ictal periods, the final ictal period (the final 5 seconds of an event) and postictal periods (up to 5 seconds after the offset of an event). Correlation values across peri-ictal periods were then compared using a one-way, repeated measures, ANOVA.

Presentation of data and statistical analyses

Data are presented as mean +/- SEM. Significance of cerebellar modulation relative to electrographic seizure events was determined by comparing the mean cerebellar ΔF/F 1.5-1 seconds prior to event onset to the mean cerebellar ΔF/F at event onset (0.5 seconds pre event onset to event onset) using Wilcoxon signed rank tests. A similar approach was used to determine significant changes in cerebellar modulation at event offset, with the pre window being 1.5-1 seconds prior to event offset, and the offset window being the 0-0.5 seconds around event offset. For peri-IED responses, the significance of modulation was determined by comparing the mean cerebellar ΔF/F in the 250 msec before an IED to that 250 msec after an IED using Wilcoxon signed rank tests.

Acknowledgments

This work was supported in part by NIH K99NS121274 (MLS), NIH R01-NS112518 (EKM), P30 DA048742 (TJE), an American Epilepsy Society Postdoctoral Fellowship (MLS), NIH R01NS111028 (TJE), RF1 NS126044 (TJE), and a University of Minnesota McKnight Land-Grant Professorship award (EKM).

Supplementary Figures

Supplementary Figure 1.

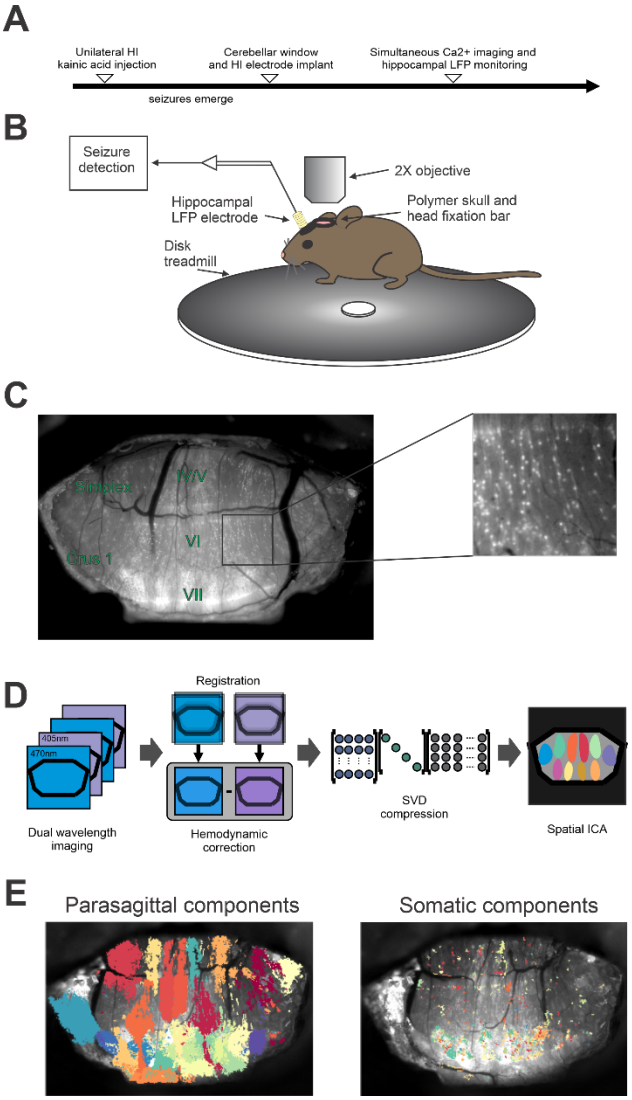

Supplementary Figure 1. See-Shell technology allows chronic widefield imaging of the cerebellum in chronically epileptic animals.

A. Experimental timeline. Animals were first injected with kainic acid into the dorsal hippocampus, to induce temporal lobe epilepsy (TLE). The unilateral, dorsal, intrahippocampal kainate model of TLE was chosen as it avoids direct chemical effects on the cerebellum, has a high rate of electrographic seizure events but also (at a much lower rate) seizures which include overtly behavioral components, has a low acute mortality rate (though a subset of animals experience SUDEP events during the chronic phase of the disease), and recapitulates key features of human unilateral mesial TLE with hippocampal sclerosis, including cell death and granule cell dispersion [24-26,34]. Animals were then implanted an electrode into the dorsal hippocampus near the original site of kainate injection, to record hippocampal epileptiform

activity during the chronic phase of the disorder. Animals were additionally implanted with a cranial window over the cerebellum using a modification of See-Shell technology, to allow for concurrent, longitudinal, cerebellar imaging. **B.** During imaging sessions, the animal was headfixed on a freely spinning disk treadmill, the hippocampal LFP was recorded, and aligned to the widefield cerebellar imaging. **C.** The cerebellar imaging window allowed simultaneous one-photon (1P) imaging of a large area of the cerebellar dorsal cortex, including Vermis lobules IV-VII, Simplex, and Crus I. Inset: The calcium indicator GCaMP6s was expressed selectively in Purkinje cells by crossing a B6.Cg-Tg(Pcp2-cre)3555Jdhu/J (Jax #010536) [21] with B6.Cg-Igs7tm162.1(tetO-GCaMP6s,CAG-tTA2)Hze/J (Jax # 031562) [22]. The resulting sparse expression in Purkinje cells allowed, even with 1P imaging, imaging of individual Purkinje cell somata. Note also that as 1P imaging was employed, in addition to simultaneously imaging a large area of the cerebellar cortex, we were also able to simultaneously image both somatic and dendritic components of Purkinje cells. **D.** Interleaved dual wavelength imaging (470nm for calcium-dependent signals, 405nm for isosbestic control) and registration of acquired images allowed for correction of movement and hemodynamic changes.[35-37] Following SVD compression, data was separated into spatial independent components (sICA; a blind source separation algorithm [23,36,41-43]), which resulted in parasagittal domains (likely driven by dendritic calcium signals[23,47-51]) and somatic domains. **E.** An example animal's parasagittal and somatic components.

Supplementary Figure 2.

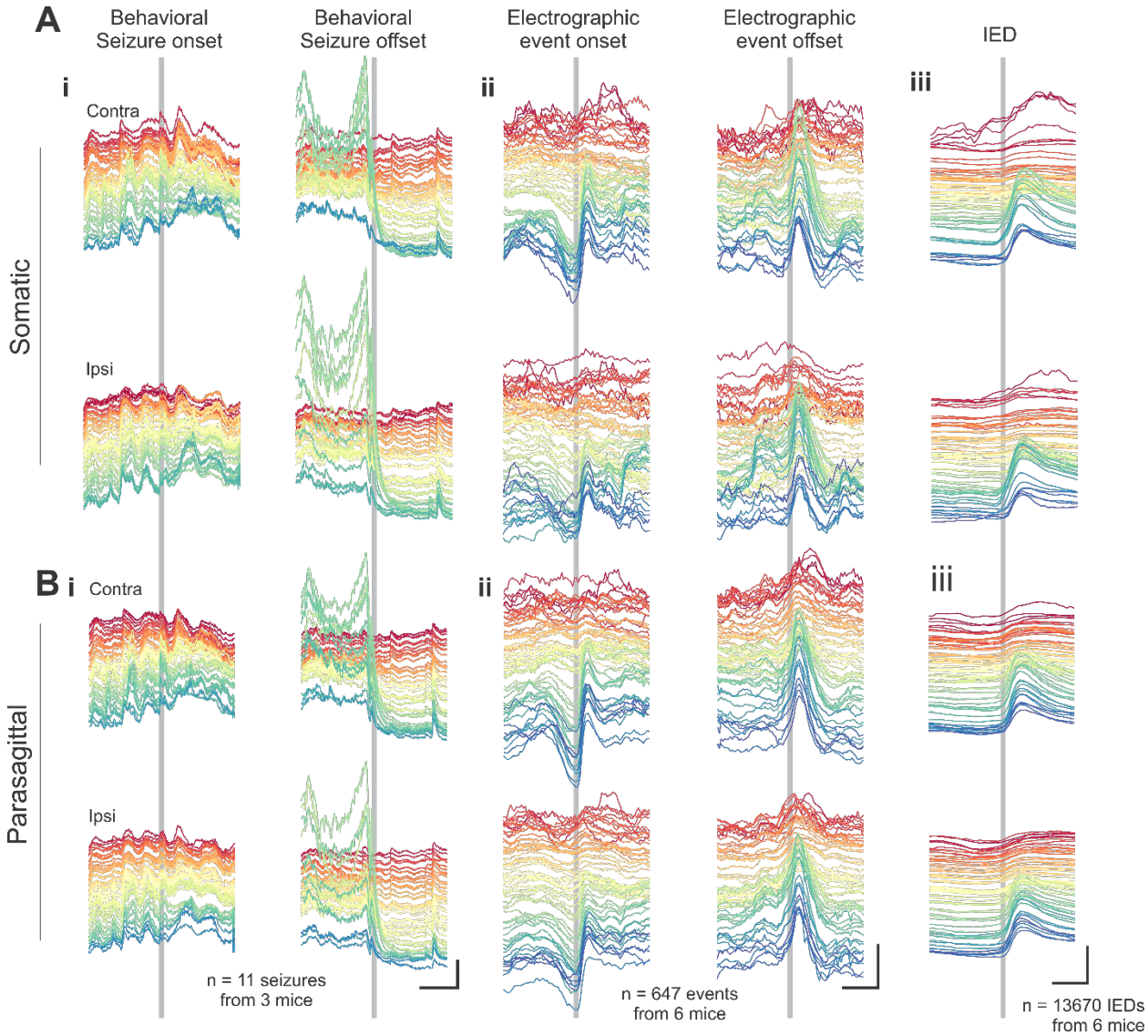

Supplementary Figure 2. Observed changes in calcium signals occur in both parasagittal domains and somatic domains.

Average calcium signals by cerebellar area (warm colors indicate more anterior cerebellum) for contralateral (top) or ipsilateral (bottom) somatic (**A**) or parasagittal (**B**) domains for seizures with an overt behavioral component (**i**), electrographic seizures without any overt behavioral component (**ii**), or IEDs (**iii**). Scale bars: i: 20% change in ΔF/F, 5s; ii: 2%, 1s; iii: 2%, 0.5s. Note that previous work has imaged in zebrafish, including the cerebellum, during acute, 4-AP or PTZ (pentylenetetrazole)-evoked, seizures[15-17], with a noted preictal and ictal increase in active neurons the cerebellum[17] (compare to panels Ai and Bi). Note also that prior work using EEG-fMRI in temporal lobe epilepsy patients found an increase in blood-oxygen-level dependent (BOLD) responses in areas including the cerebellar cortex[52], in keeping with the large rebound we find in cerebellar calcium signals immediately following a hippocampal IED

(panels Aiii and Biii). The temporal resolution of BOLD imaging may have prevented detection of a smaller pre-IED decrease in cerebellar activity. While our work has focused on the cerebellum during hippocampal epileptiform events in a model of TLE, the cerebellum may be more widely relevant to the epilepsies. Changes in the cerebellum during IEDs have also been noted in other patient populations and studies[53], including frontal lobe epilepsy patients[52]. Note also that other areas may show preictal changes in other models of epilepsy. This includes changes in superior colliculus activity prior to seizures in a rat model of absence epilepsy[54], increased preictal activity in neocortical somatostatin-expressing neurons and a deficit in parvalbumin-interneuron synchronization in heat-induced seizures in a mouse model of Dravet syndrome[10,11], and a preictal appearance of superhubs in pentylenetetrazol-treated zebrafish[1].

Supplementary Figure 3.

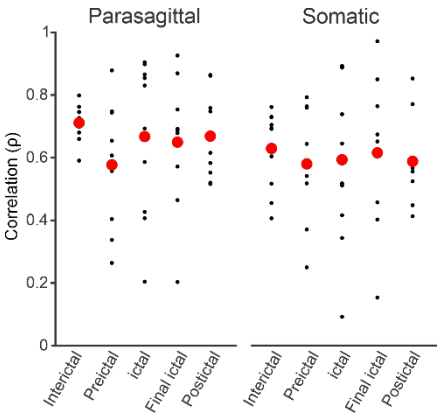

Supplementary Figure 3. Behavioral seizures are not associated with widespread increases in correlated cerebellar activity. Correlations in calcium activity across ICs (left, parasagittal; right, somatic) were calculated for each behavioral seizure event for the surrounding interictal period, the preictal period, the ictal period (excluding the final 5s), the final ictal period (final 5s before seizure offset), and the immediate postictal (5s) period. There was no significant change in the average correlations for parasagittal ($p=0.63$, repeated measures ANOVA; $p>0.05$ for all pairwise comparisons, Wilcoxons) nor the somatic domains ($p=0.69$, repeated measures ANOVA; $p>0.05$ for all pairwise comparisons, Wilcoxons). Each block dot represents data from one behavioral seizure event. Each red dot represents the mean across seizures.

Supplementary Figure 4.

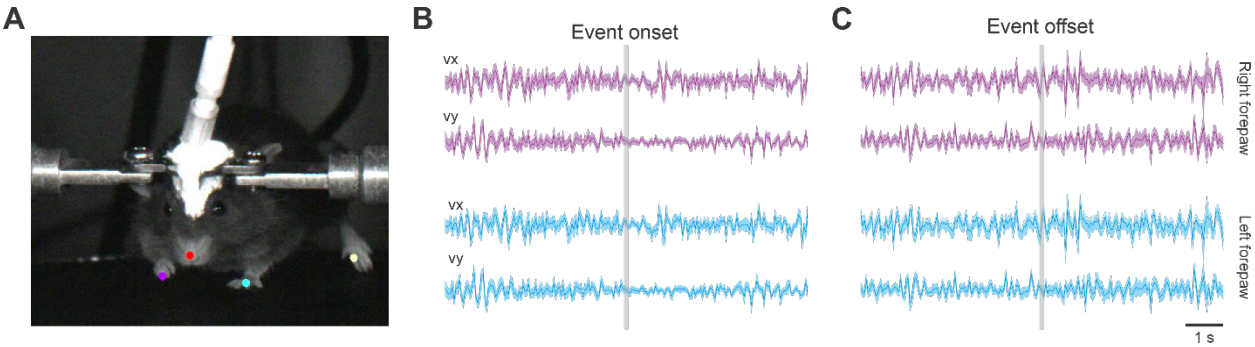

Supplementary Figure 4. Lack of noticeable forelimb alteration during electrographic-only seizure events. A. DeepLabCut [40] markerless tracking allowed automated tracking of the right (purple) and left (blue) forepaws during imaging sessions. **B-C**. Electrographic seizures were not associated with any notable changes in the movement of either forepaw, at seizure onset (B) nor seizure offset (C). Shown is relative position for each paw in the video image for the x (vx, top) or y (vy, bottom) axes. Shading represents SEM. Data represents paw location data for 244 electrographic seizure events from 6 animals. Scale bar: 1s.

Supplementary Figure 5.

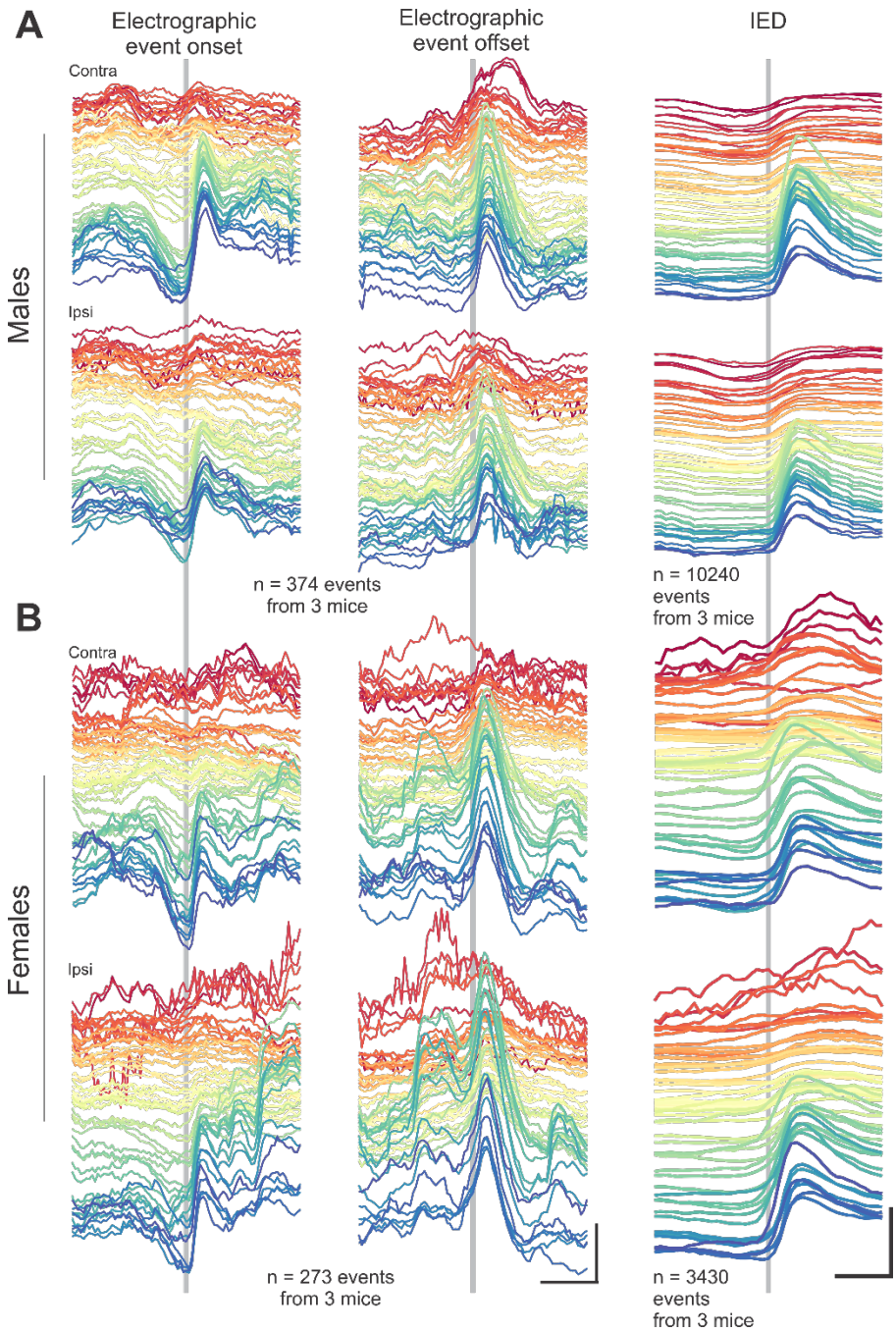

Supplementary Figure 5. Both male and female animals show a similar cerebellar response profile to hippocampal epileptiform events.

Average cerebellar responses by cerebellar region (top: contralateral, bottom: ipsilateral cerebellum; warmer colors represent more anterior regions) for male (A) and female (B) animals aligned to electrographic seizure onset (left), offset (middle), or IED peak (right). Note that the pre-ictal decrease, the post-ictal rebound, and the initial slight-dip followed by large post-IED rebound is visible for both male and female animals. Scale bars: 1 second, 2% ΔF/F.

Supplementary Video 1. Cerebellar modulation around a spontaneous, overt behavioral seizure.

Widefield cerebellar imaging stack captured during the spontaneous behavioral seizure in **Figure 1A**. Top left panel is the hippocampal LFP recorded during the entire stack, bottom left panel is a zoomed in view of the real time hippocampal LFP aligned to the imaging stack. Note the increased, bilateral activation of the cerebellum beginning several seconds prior to the high amplitude spiking of the behavioral seizure, the sustained posterior activation during the seizure, and the depression beginning in anterior regions of the cerebellum prior to seizure offset. Bright postictal flashes are also apparent with concurrent postictal spikes in the hippocampal LFP.

Supplementary References

1. Hadjiabadi, D. & Soltesz, I. From single-neuron dynamics to higher-order circuit motifs in control and pathological brain networks. *The Journal of physiology* (2022).
2. Rossi, L.F., Wykes, R.C., Kullmann, D.M. & Carandini, M. Focal cortical seizures start as standing waves and propagate respecting homotopic connectivity. *Nature communications* **8**, 217 (2017).
3. Aeed, F., Shnitzer, T., Talmon, R. & Schiller, Y. Layer- and Cell-Specific Recruitment Dynamics during Epileptic Seizures In Vivo. *Annals of neurology* **87**, 97-115 (2020).
4. Montgomery, M.K*., et al.* Glioma-Induced Alterations in Neuronal Activity and Neurovascular Coupling during Disease Progression. *Cell Rep* **31**, 107500 (2020).
5. Lau, L.A., Staley, K.J. & Lillis, K.P. In vitro ictogenesis is stochastic at the single neuron level. *Brain : a journal of neurology* **145**, 531-541 (2022).
6. Lillis, K.P*., et al.* Evolution of Network Synchronization during Early Epileptogenesis Parallels Synaptic Circuit Alterations. *The Journal of neuroscience : the official journal of the Society for Neuroscience* **35**, 9920-9934 (2015).
7. Meyer, J., Maheshwari, A., Noebels, J. & Smirnakis, S. Asynchronous suppression of visual cortex during absence seizures in stargazer mice. *Nature communications* **9**, 1938 (2018).
8. Khoshkhoo, S., Vogt, D. & Sohal, V.S. Dynamic, Cell-Type-Specific Roles for GABAergic Interneurons in a Mouse Model of Optogenetically Inducible Seizures. *Neuron* **93**, 291-298 (2017).
9. Berdyyeva, T.K*., et al.* Direct Imaging of Hippocampal Epileptiform Calcium Motifs Following Kainic Acid Administration in Freely Behaving Mice. *Frontiers in neuroscience* **10**, 53 (2016).
10. Somarowthu, A., Goff, K.M. & Goldberg, E.M. Two-photon calcium imaging of seizures in awake, head-fixed mice. *Cell Calcium* **96**, 102380 (2021).
11. Tran, C.H*., et al.* Interneuron Desynchronization Precedes Seizures in a Mouse Model of Dravet Syndrome. *The Journal of neuroscience : the official journal of the Society for Neuroscience* **40**, 2764-2775 (2020).
12. Liebergall, S.R. & Goldberg, E.M. Ndnf Interneuron Excitability Is Spared in a Mouse Model of Dravet Syndrome. *The Journal of neuroscience : the official journal of the Society for Neuroscience* **44**(2024).
13. Mattis, J*., et al.* Corticohippocampal circuit dysfunction in a mouse model of Dravet syndrome. *Elife* **11**(2022).
14. Goff, K.M., Liebergall, S.R., Jiang, E., Somarowthu, A. & Goldberg, E.M. VIP interneuron impairment promotes in vivo circuit dysfunction and autism-related behaviors in Dravet syndrome. *Cell Rep* **42**, 112628 (2023).
15. Rosch, R.E., Hunter, P.R., Baldeweg, T., Friston, K.J. & Meyer, M.P. Calcium imaging and dynamic causal modelling reveal brain-wide changes in effective connectivity and synaptic dynamics during epileptic seizures. *PLoS Comput Biol* **14**, e1006375 (2018).
16. Liu, J. & Baraban, S.C. Network Properties Revealed during Multi-Scale Calcium Imaging of Seizure Activity in Zebrafish. *eNeuro* **6**(2019).
17. Diaz Verdugo, C*., et al.* Glia-neuron interactions underlie state transitions to generalized seizures. *Nature communications* **10**, 3830 (2019).
18. Bando, Y., Wenzel, M. & Yuste, R. Simultaneous two-photon imaging of action potentials and subthreshold inputs in vivo. *Nature communications* **12**, 7229 (2021).
19. Wenzel, M., Hamm, J.P., Peterka, D.S. & Yuste, R. Acute Focal Seizures Start As Local Synchronizations of Neuronal Ensembles. *The Journal of neuroscience : the official journal of the Society for Neuroscience* **39**, 8562-8575 (2019).

20. Shuman, T.*, et al.* Breakdown of spatial coding and interneuron synchronization in epileptic mice. *Nature neuroscience* **23**, 229-238 (2020).
21. Zhang, X.M.*, et al.* Highly restricted expression of Cre recombinase in cerebellar Purkinje cells. *Genesis* **40**, 45-51 (2004).
22. Daigle, T.L.*, et al.* A Suite of Transgenic Driver and Reporter Mouse Lines with Enhanced Brain-Cell-Type Targeting and Functionality. *Cell* **174**, 465-480 e422 (2018).
23. Streng, M.L.*, et al.* Mesoscale Ca2+ imaging reveals networks of Purkinje cell dendritic and somatic modulation, with divergent roles of activity versus correlation during behavior. *bioRxiv*, 2023.2010.2005.561090 (2023).
24. Cavalheiro, E.A., Riche, D.A. & Le Gal La Salle, G. Long-term effects of intrahippocampal kainic acid injection in rats: a method for inducing spontaneous recurrent seizures. *Electroencephalography and clinical neurophysiology* **53**, 581-589 (1982).
25. Bouilleret, V.*, et al.* Recurrent seizures and hippocampal sclerosis following intrahippocampal kainate injection in adult mice: electroencephalography, histopathology and synaptic reorganization similar to mesial temporal lobe epilepsy. *Neuroscience* **89**, 717-729 (1999).
26. Bragin, A., Engel, J., Jr., Wilson, C.L., Vizentin, E. & Mathern, G.W. Electrophysiologic analysis of a chronic seizure model after unilateral hippocampal KA injection. *Epilepsia* **40**, 1210-1221 (1999).
27. Krook-Magnuson, E., Armstrong, C., Oijala, M. & Soltesz, I. On-demand optogenetic control of spontaneous seizures in temporal lobe epilepsy. *Nature communications* **4**, 1376 (2013).
28. Streng, M.L. & Krook-Magnuson, E. Excitation, but not inhibition, of the fastigial nucleus provides powerful control over temporal lobe seizures. *The Journal of physiology* **598**, 171-187 (2020).
29. Streng, M.L., Tetzlaff, M.R. & Krook-Magnuson, E. Distinct Fastigial Output Channels and Their Impact on Temporal Lobe Seizures. *The Journal of neuroscience : the official journal of the Society for Neuroscience* **41**, 10091-10107 (2021).
30. Bar-Klein, G.*, et al.* Isoflurane prevents acquired epilepsy in rat models of temporal lobe epilepsy. *Annals of neurology* **80**, 896-908 (2016).
31. Riban, V.*, et al.* Evolution of hippocampal epileptic activity during the development of hippocampal sclerosis in a mouse model of temporal lobe epilepsy. *Neuroscience* **112**, 101-111 (2002).
32. Klein, S., Bankstahl, J.P., Loscher, W. & Bankstahl, M. Sucrose consumption test reveals pharmacoresistant depression-associated behavior in two mouse models of temporal lobe epilepsy. *Experimental neurology* **263**, 263-271 (2015).
33. Levesque, M. & Avoli, M. The kainic acid model of temporal lobe epilepsy. *Neurosci Biobehav Rev* **37**, 2887-2899 (2013).
34. Zeidler, Z.*, et al.* Targeting the Mouse Ventral Hippocampus in the Intrahippocampal Kainic Acid Model of Temporal Lobe Epilepsy. *eNeuro* **5**(2018).
35. Jacobs, E.A.K., Steinmetz, N.A., Peters, A.J., Carandini, M. & Harris, K.D. Cortical State Fluctuations during Sensory Decision Making. *Current biology : CB* **30**, 4944-4955 e4947 (2020).
36. West, S.L.*, et al.* Wide-Field Calcium Imaging of Dynamic Cortical Networks during Locomotion. *Cereb Cortex* **32**, 2668-2687 (2022).
37. MacDowell, C.J. & Buschman, T.J. Low-Dimensional Spatiotemporal Dynamics Underlie Cortex-wide Neural Activity. *Current biology : CB* **30**, 2665-2680 e2668 (2020).
38. Stieve, B.J., Richner, T.J., Krook-Magnuson, C., Netoff, T.I. & Krook-Magnuson, E. Optimization of closed-loop electrical stimulation enables robust cerebellar-directed seizure control. *Brain : a journal of neurology* (2022).
39. Stieve, B.J., Smith, M.M. & Krook-Magnuson, E. LINCs Are Vulnerable to Epileptic Insult and Fail to Provide Seizure Control via On-Demand Activation. *eNeuro* **10**(2023).

40. Mathis, A.*, et al.* DeepLabCut: markerless pose estimation of user-defined body parts with deep learning. *Nature neuroscience* **21**, 1281-1289 (2018).
41. Nietz, A.K.*, et al.* To be and not to be: wide-field Ca2+ imaging reveals neocortical functional segmentation combines stability and flexibility. *Cereb Cortex* (2023).
42. Makino, H.*, et al.* Transformation of Cortex-wide Emergent Properties during Motor Learning. *Neuron* **94**, 880-890 e888 (2017).
43. Musall, S., Kaufman, M.T., Juavinett, A.L., Gluf, S. & Churchland, A.K. Single-trial neural dynamics are dominated by richly varied movements. *Nature neuroscience* **22**, 1677-1686 (2019).
44. Ren, C. & Komiyama, T. Characterizing Cortex-Wide Dynamics with Wide-Field Calcium Imaging. *The Journal of neuroscience : the official journal of the Society for Neuroscience* **41**, 4160-4168 (2021).
45. Couto, J.*, et al.* Chronic, cortex-wide imaging of specific cell populations during behavior. *Nature protocols* **16**, 3241-3263 (2021).
46. Saxena, S.*, et al.* Localized semi-nonnegative matrix factorization (LocaNMF) of widefield calcium imaging data. *PLoS Comput Biol* **16**, e1007791 (2020).
47. Michikawa, T.*, et al.* Distributed sensory coding by cerebellar complex spikes in units of cortical segments. *Cell Rep* **37**, 109966 (2021).
48. Kostadinov, D., Beau, M., Blanco-Pozo, M. & Hausser, M. Predictive and reactive reward signals conveyed by climbing fiber inputs to cerebellar Purkinje cells. *Nature neuroscience* **22**, 950-962 (2019).
49. Heffley, W.*, et al.* Coordinated cerebellar climbing fiber activity signals learned sensorimotor predictions. *Nature neuroscience* **21**, 1431-1441 (2018).
50. Ozden, I., Sullivan, M.R., Lee, H.M. & Wang, S.S. Reliable coding emerges from coactivation of climbing fibers in microbands of cerebellar Purkinje neurons. *The Journal of neuroscience : the official journal of the Society for Neuroscience* **29**, 10463-10473 (2009).
51. Schultz, S.R., Kitamura, K., Post-Uiterweer, A., Krupic, J. & Hausser, M. Spatial pattern coding of sensory information by climbing fiber-evoked calcium signals in networks of neighboring cerebellar Purkinje cells. *The Journal of neuroscience : the official journal of the Society for Neuroscience* **29**, 8005-8015 (2009).
52. Fahoum, F., Lopes, R., Pittau, F., Dubeau, F. & Gotman, J. Widespread epileptic networks in focal epilepsies: EEG-fMRI study. *Epilepsia* **53**, 1618-1627 (2012).
53. Wiest, R.*, et al.* Widespread grey matter changes and hemodynamic correlates to interictal epileptiform discharges in pharmacoresistant mesial temporal epilepsy. *J Neurol* **260**, 1601-1610 (2013).
54. Campos-Rodriguez, C., Palmer, D. & Forcelli, P.A. Optogenetic stimulation of the superior colliculus suppresses genetic absence seizures. *Brain : a journal of neurology* **146**, 4320-4335 (2023).